Geological Modeling of Hydrocarbon Reservoir Rocks in the Mafia Basin, Offshore Tanzania

Bahati Mohamed, Elisante Mshiu and Ernest Mulaya
Geology Department, University of Dar es Salaam, P. O. Box 35052 Dar es Salaam, Tanzania
Corresponding author e-mail: mshiutz@gmail.com

Abstract
This study presents a 3D geological model of reservoir rocks in the Mafia Basin based on interpretation of 2D seismic and well data towards understanding the hydrocarbon prospectivity. 2D seismic data were used to generate surface maps and therefore the subsurface configuration of the reservoir complemented with petrophysical analysis to determine lithology and reservoir properties. Structural and petrophysical properties modeling were distributed stochastically within the constructed 3D grid using Sequential Indicator Simulation (SIS) and Gaussian Random Function Simulation (GRFS) algorithms. Results from well log analysis and petrophysical models classify the reservoir under a moderate reservoir quality with 19% to 20% porosity, 6–7 mD permeability and 60% to 65% water saturation. The observed high values of water saturation imply that the hydrocarbon accumulation in the mapped area is insignificant. The reservoir structural model and subsurface configuration shows stratigraphical trap as the only trapping mechanism in the area.. However, 3D seismic and multiple wells are needed for effective correlation of geological information to enhance the structural configuration and lateral continuity of the reservoir.

Keywords: Geological modeling, Mafia basin, 2D seismic data, reservoir rocks

Introduction

Block 5 is one of the exploration blocks in Tanzania, which is within the Mafia Deep Offshore Sedimentary Basin (Kent et al. 1971, Alvarenga et al. 2012). The basin is an exploration area with a great potential of hydrocarbon resources as revealed by large number of hydrocarbon discoveries (Petzet 2012, Zongying et al. 2013). These huge hydrocarbon discoveries in offshore Mafia basin call for static reservoir modeling to be conducted and used for a better understanding of the block prospectivity by integrating and reconcile all the available data towards the development stage (Harris 1975).

A reservoir model presents the physical space of the reservoir by a group of discrete cells, defined by a grid which may be regular or irregular (Branets et al. 2009). The group of cells is usually three-dimensional, although 1D and 2D models are sometimes used. Values for attributes such as porosity, permeability and water saturation are associated with each cell, and it is indirectly estimated to apply uniformly throughout the volume of the reservoir represented by the cell (Pyrcz and Deutsch 2014). Reservoir modeling involves transfer of the available subsurface data and knowledge into a digital (computerized) numerical representation of the subsurface (Bjorlykke 2010). Generally, this can be achieved through extrapolating the available data to the entire volume of interest which is now considered an essential part of understanding and developing oil and gas resources (Bjorlykke 2010). A broad understanding of a reservoir is best captured in a 3D geological model (Christie and Blunt 2001, Nikravesh and Aminzadeh 2001, Harris and Weber 2006). This study uniquely produces the 3D geological reservoir models

of the Mafia Basin towards understanding its hydrocarbon prospectivity. This involves describing the spatial distribution of the litho-

types with different petrophysical parameters of the offshore Block 5 in Tanzania.
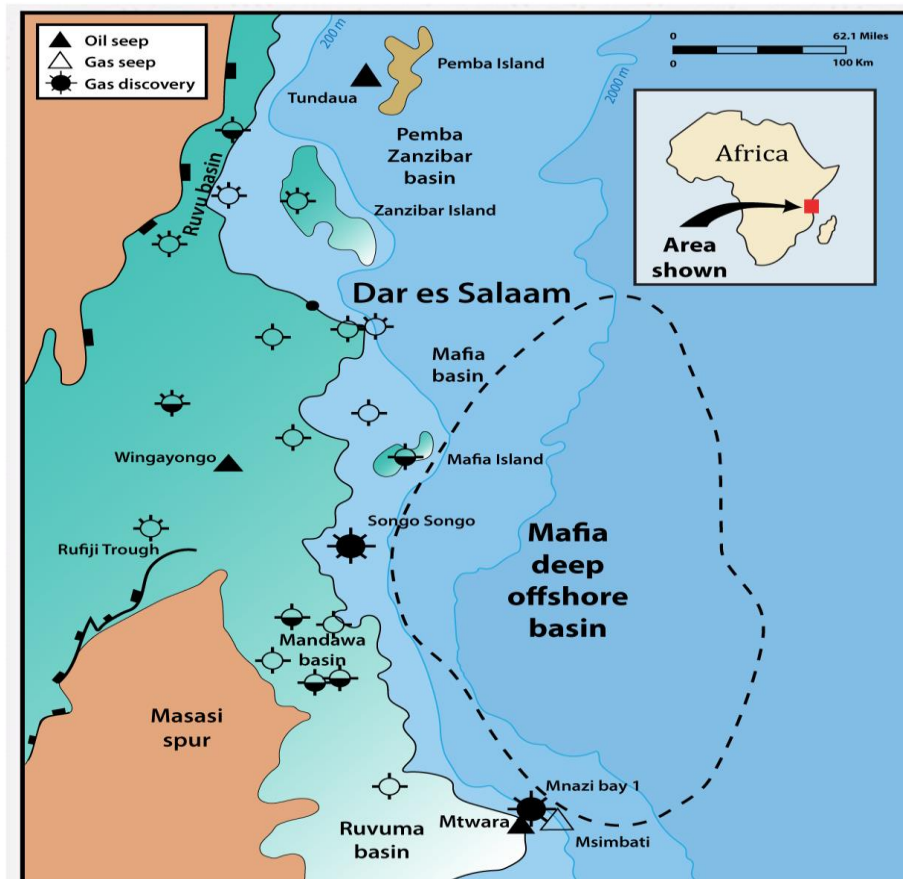
Figure 1: A simplified map showing the location of Mafia offshore basin adapted from Cope (2000).

Geology of the study area

Offshore Mafia Basin is located 200 km east of the coastal Tanzania in the Indian Ocean at a water depth of about 500 m to 3000 m (Figure 1, Kent et al. 1971, Cope 2000, Alvarenga et al. 2012). The offshore sedimentary rocks of Tanzania were influenced by contemporarily regional extensional tectonics (Nicholas et al. 2007). They are dominated by carbonate deposition which prevailed in the Jurassic period (Kent et al. 1971). The Lower Cretaceous Neocomian epoch had significant

sedimentary input of sand due to lower sea levels and/or tectonic uplift of sediment source areas (Cope 2000, Petrobras 2013). Neocomian to Maastrichtian deposition was predominately composed of deep water shales across the Mafia Deep Basin (Alvarenga et al. 2012). Significant submarine slumps and slides occurred during the Turonian and the later Maastrichtian unconformity identified in onshore wells is linked to a high sediment input to the deeper parts of the basin (Zongying et al. 2013). This is probably caused by tectonic activities

and/or sea level drop. Records of Lower Eocene depositional environment point out to a carbonate platform in the region of the Mafia Island and siliciclastic deposited in the adjacent lows (Alvarenga et al. 2012, Cope 2000). Oligocene and Miocene offshore deposition had a strong deltaic influence as a result of increased sediment input from the Rufiji and Ruvuma delta (McDonough et al. 2013). Regional tectono-stratigraphic history of the area favors the potential hydrocarbon generation, migration and accumulation (Slind et al. 1998, Pereira-Rego et al. 2013).

The well reservoir was inferred to have been deposited as a gravity flow in a deep water environment (Figure 2, Petrobras 2013). Post drilling data and sidewall core analysis point out to deposition of discrete channels followed by amalgamated channel deposits on the slope, pelitic sediments form the top and lateral seals, therefore a typical stratigraphic target, located on a ramp with no associated structural features (Alvarenga et al. 2012).
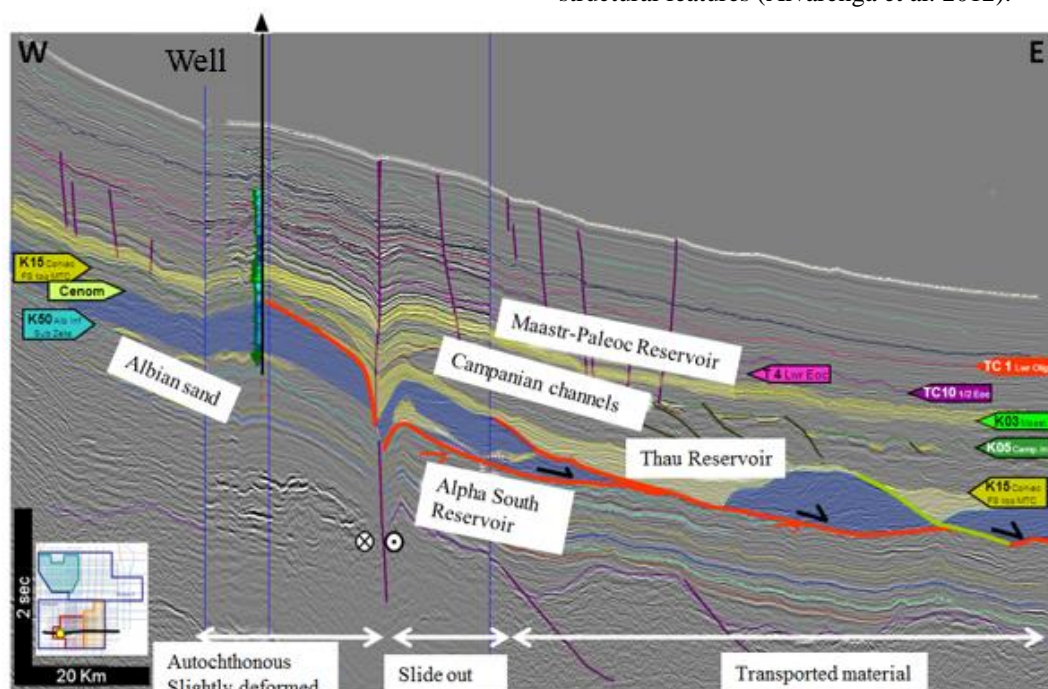
Figure 2: Seismic interpretation of the main reservoir units of the Cretaceous-Cenozoic time span on a west-east seismic section (Petrobras 2013).

Materials and Methods

Seismic datasets used were obtained from Tanzania Petroleum Development Corporation (TPDC), which include six SEG-Y format 2D seismic lines and one available exploration well from the Mafia basin. Procedures used in the modeling process include integrating petrophysics parameters and seismic data to provide the range of lithotypes, rock properties and geostatistical inversion to determine a set of reasonable seismic-derived rock property and structural elements (Farmer 2005, Merletti and Torres-Verdin 2006). Correlation of wells with seismic section was performed through synthetic seismograms from wells based on the best visual match of package reflection events between the synthetic seismogram and the actual seismic sections (Cunningham and Droxler 2000). The resulting mix of

interpreted seismic surfaces, faults and calculated intermediate horizons from well correlation and isochores make the geological framework, which can be considered as the most precise model of the structural elements that is usually in two-way travel time domain (Bjorlykke 2010).

The static reservoir model was constructed by using Petrel[TM] version 2014 software applications in two main steps following Petrel help manual version (Schlumberger 2014). The first step was structural 3D grid modeling followed by 3D grid property modeling whose flow model is summarized in Figure 3 below.
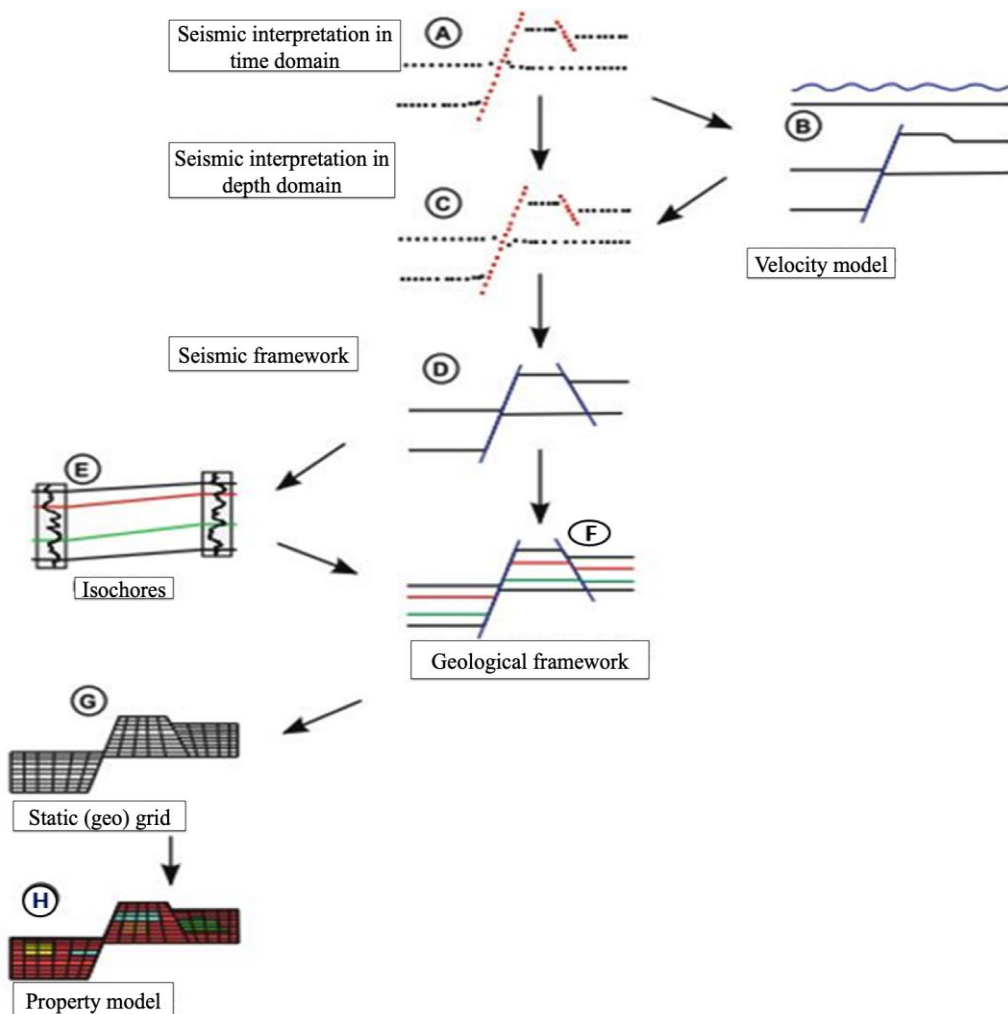
Figure 3: Reservoir model construction workflow (after Bjorlykke 2010).

Seismic interpretation and 3D grid modeling

The construction of a 3D structural grid started with seismic interpretation by identification and picking of top and base horizons of a reservoir (Gluyas and Swarbrick 2003, Soleimani and Shokri 2015). These were defined after tying the

well tops onto respective reflectors on a seismic section through seismic well tie process using well data and checkshot survey from the well (Deutsch 1992, Figure. 4).
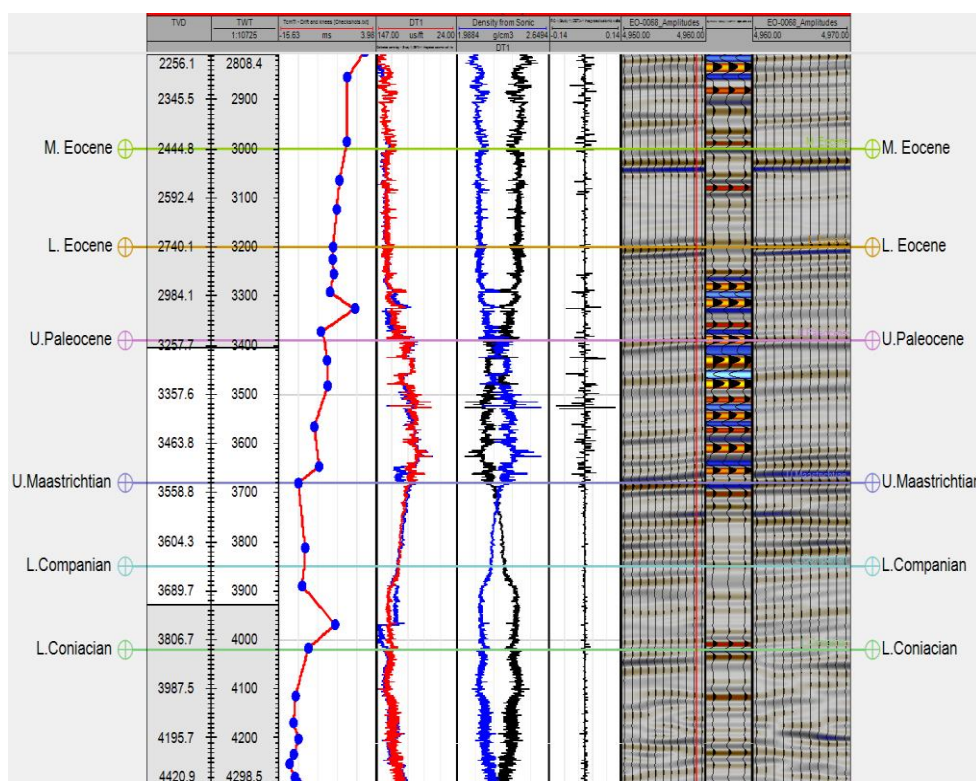
Figure 4: Integrated sonic calibration and seismic well tie processes. Depth tracks in TVD and TWT, checkshot points, original (blue) and calibrated sonic (red) logs, calibrated sonic (blue) and density (black) logs for synthetic, reflection coefficient, left seismic reference, synthetic seismogram, and right seismic reference from track 1 to 9, respectively.

Structural surface maps of the top and base of the reservoir were generated from the picked horizons using a convergent interpolation algorithm which is used to generate surface maps by retaining general trends in areas with little data and honors more details in areas where more data exists. The generated maps were domain converted from time to depth by using a velocity model and used as primary input into constructing a simple geological framework. The geological framework was gridded by 50 m x 50 m grid size based on the size and geological nature of the reservoir body to create a volume of Geo-grid model prior to petrophysical properties population (Ringrose and Bentley 2015, Soleimani and Shokri 2015).

Petrophysical and lithology evaluation

A detailed petrophysical evaluation was conducted for well log data by using scientific equations and models, whereby output curves for volume of shale, porosity, water saturation and permeability were generated. The volume of shale curve was determined from gamma ray log using a cut off of 35 API for gamma

ray matrix and 100 API for gamma ray shale. Porosity curve was estimated by plotting neutron porosity log against bulk density log using Schlumberger charts assuming density of the fluid is 1.0 gm/cm³.

Water saturation curve was estimated using Archie's equation under the assumption that; a = lithology constant = 1; n = saturation exponent = 2; m = cementation factor = 2; R_w = water resistivity; R_t = formation resistivity; $\emptyset$ = porosity and S_W = water saturation (Archie 1942, equation 1).

$$S_W = \left[\frac{a * R_w}{\emptyset^m * R_t}\right]^{\frac{1}{n}} \qquad (1)$$

Apparent water resistivity (R_{wa}) was first determined from the calculated R_w log of a clean water bearing formation by equating Archie's equation assuming $R_w = R_t$ and S_W =1 in a wet fully flushed zone (Archie1942, equation 2).

$$Rwa = \emptyset^2 * Rt \qquad (2)$$

Permeability curve was determined by using Timur model parameters on Wyllie-Rose equation that takes porosity and water saturation into account (Timur 1968). Wyllie-Rose permeability equation is an equation derived from laboratory core calibration (Timur 1968, equation 3);

$$K = K_w * \left(\frac{Q^d}{sw^e}\right) \qquad (3)$$

where d = porosity exponent, e = irreducible water saturation exponent, K_W = permeability constant, Φ = porosity, S_w = irreducible water saturation, and K = permeability.

The Timur model parameters and exponents defined by Timur (1968) based on laboratory core analysis studies were; K_w = Permeability constant = 3400 for oil and 340 for gas, d = Porosity exponent = 4.4 and e = irreducible water saturation exponent = 2. Lithology log was defined based on lithological logs such a gamma ray log for determination of clean and shale formations, neutron porosity and bulk density crossing behaviors for determination of lithology type and Pef (Photoelectric factor) log for direct confirmation of the lithology type. The equation (4) below based on a cut off of 35

API of gamma ray log and lithology template in Figure 5 were primarily used.

Lithology log = If (GR < 35, 0, 1) (4)

Code	Name	Parent	Background	Lines	Pattern
0	Sand				
1	Shale				

Figure 5: Lithology template with sand (sandsone) and shale codes used together with gamma ray log in the facies equation.

3D grid property modeling

A 3D property model was built by integrating the 3D grid structural model and that of the petrophysical and lithology evaluation. The gridded structural model was populated with petrophysical properties (i.e., porosity, permeability and water saturation) and lithology information using geostatistical algorithms to determine spatial distribution (Ringrose and Bentley 2015). Lithologic distribution model was determined based on the lithology curve generated from lithology evaluation. The log was up scaled into the cells and SIS (Sequential Indicator Simulation algorithm was used to populate the model with a normal distribution of the facies trend as per Seifert and Jensen (1999).

Porosity model was based on the porosity log generated from petrophysical evaluation; the log was up scaled to the layering scheme using facies as a controlling bias that ensured the values are suitable for the facies property of the cells or grids (Holden and Nielson 2000). The porosity was distributed in the model using GRFS (Gaussian Random Function Simulation) algorithm (Hu 2000). Permeability model was based on the permeability log generated from petrophysical evaluation; the log was up scaled to the layering scheme using facies and respective porosity as a controlling bias ensuring appropriate values in the cells. The property was distributed in the model zone using GRFS (Gaussian Random Function Simulation) algorithm. Water saturation model was based on the water saturation curve generated from

petrophysical evaluation. Water saturation log was up scaled to the layers using facies, porosity and permeability as controlling bias for appropriate values in the cells. The property was distributed in the model using GRFS (Gaussian Random Function Simulation) algorithm (Hu 2000).

Results
Pay zone identification and seismic interpretation
The reservoir section and the respective lithology were identified within the Albian formation at a depth between 4588 m (top target) to 4689 m (base target) (Figure 6). This

was complemented by Time-Depth Relationship (TDR) traced on seismic section by synthetic seismogram (Figure. 7). The identification is based on the presence of very low gamma ray log values less than 35 API in sand (sandstone) areas intercalated by shale in areas with high gamma ray log values more than 35 API. Also the crossover behaviors of neutron porosity log against bulk density log indicate the present of fluid bearing porous formation. The log values and crossover behaviors are considered correct since the area is confirmed not to be a washout by caliper log readings (Figure 6).
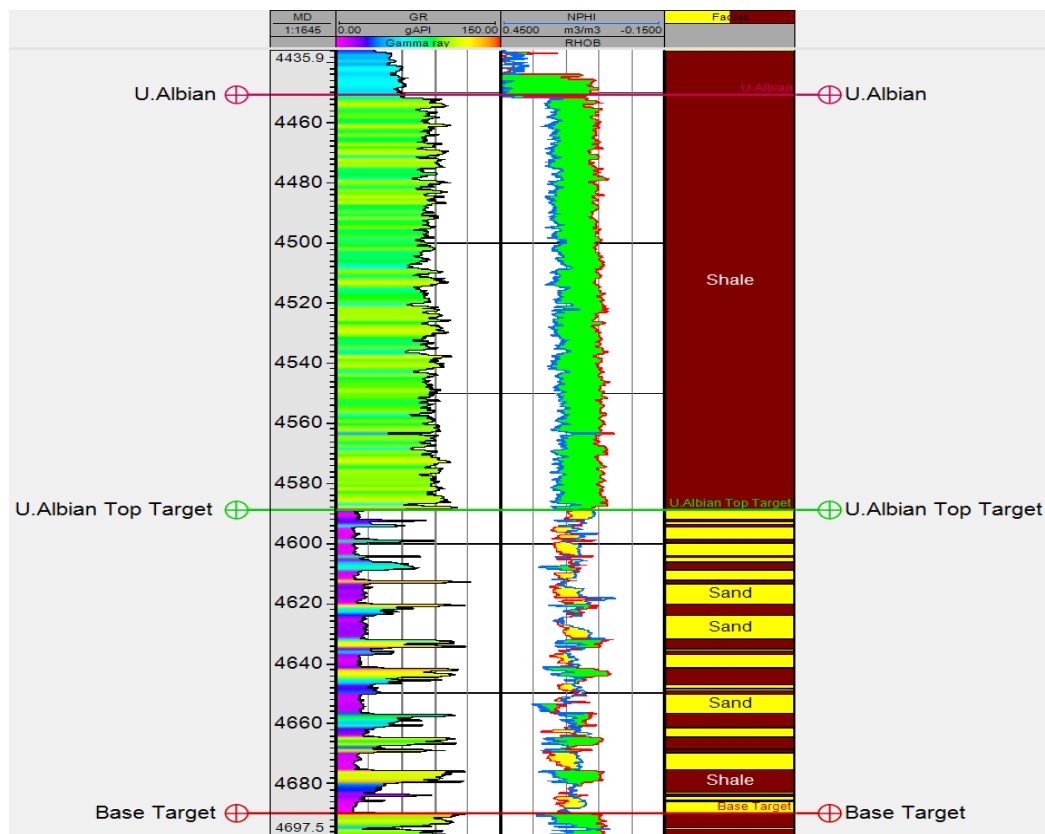
Figure 6: The studied well logs with stratigraphic breakdown, identified lithology and reservoir section in yellow.
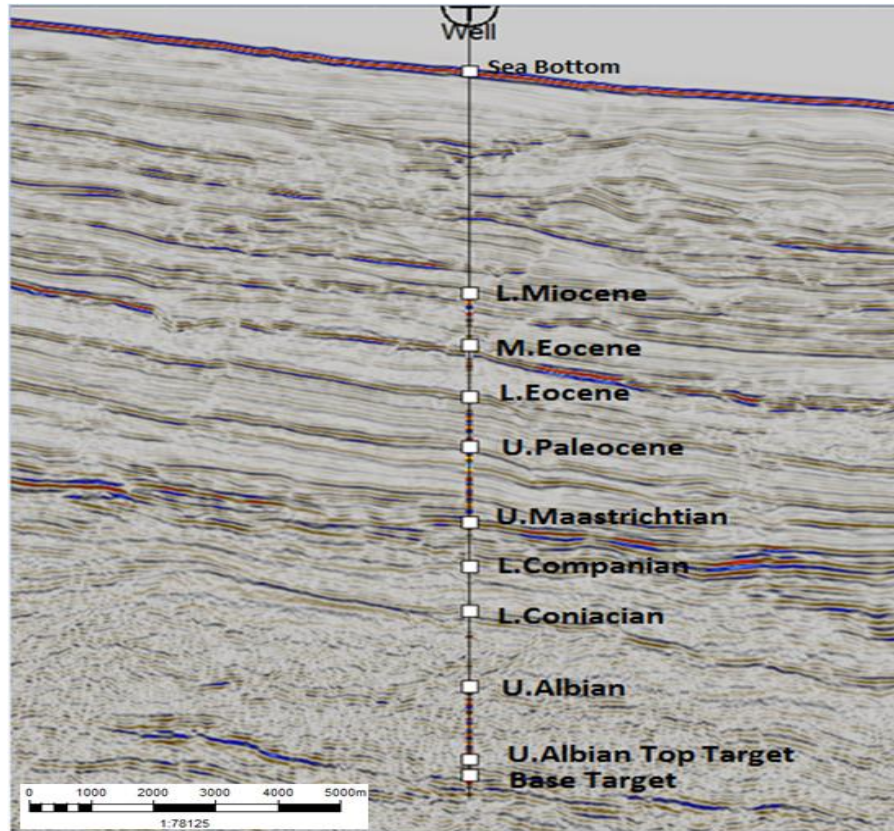
Figure 7: Overlay of synthetic seismogram log on a seismic section for tracing and mapping horizons of the corresponding well markers from well data on seismic section.

3D structural models

The interpretations from seismic data were the primary inputs for generating structural surface maps. Time structural maps of the top and base surfaces of the reservoir section are displayed in Figure 8. Maps show contour lines in time elevation from -4325 ms to -4850 ms for the top surface and -4400 ms to -4875 ms for the base surface. In both maps, the reservoir section is covering most of the elevated part around the contour lines of -4375 ms to -4625 ms indicated by the black line, while the rest of the part is a user defined boundary based on structure of the sand body (Figure 8). Better results of generated surface depend on good quality and quantity of the input data. Horizons from seismic interpretation are clean and close as possible in avoiding surfaces with picks (unclean surfaces) and enhance software extrapolation.
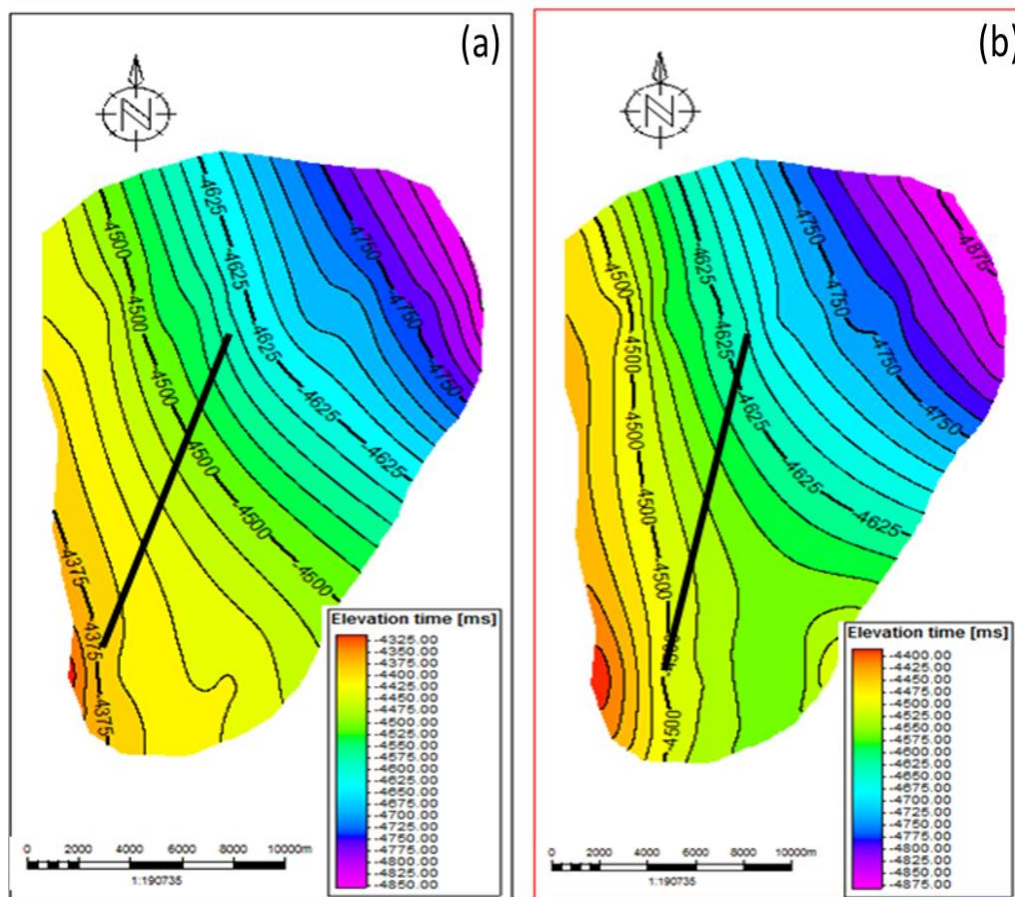
Figure 8: Time structural maps (a) top surface and (b) base surfaces with a black line indicating reservoir closure.

Velocity models

The depth conversions of the surface maps from time to depth as performed using a simple velocity model using checkshots are illustrated in Figure 9. Similar changes were observed in the northeast part of the base surface in depth from the base surface in time (Figure 10). The converted depth structural maps of the top and base surfaces of the reservoir section show contour lines in depth elevation between -4320 m to -4860 m for the top surface and -4440 m to -4920 m for the base surface (Figure 10). In both maps, the reservoir section covers most of the elevated part around the contour lines of -4320 m to -4680 m as indicated by the black line while the rest of the part is a user defined boundary based on structure of the sandstone body (Figure 10). The 3D structural model developed from structural maps in depth domain displays a 3D perspective of the reservoir section and based on the stratigraphic break down the modeled reservoir section has only one zone between the top and base surface with no faults associated with the reservoir section (Figure 11).

246
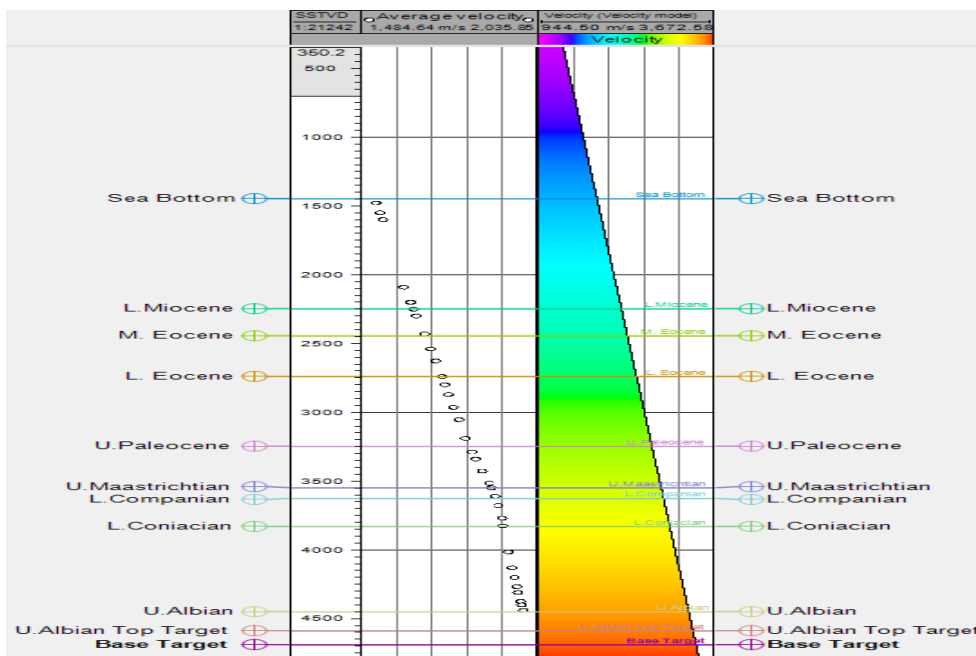
Figure 9: The interval velocity log from checkshot and velocity log from velocity model in track two and three respectively, showing the velocity model accuracy.
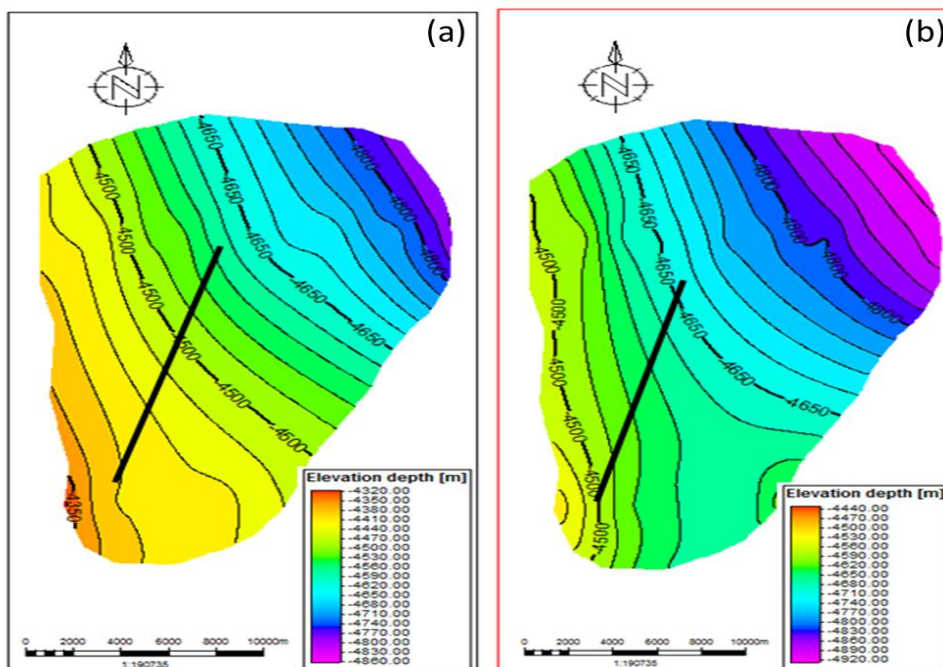
Figure 10: Depth structural map for (a) top surface and (b) base surfaces with a black line indicating reservoir closure.
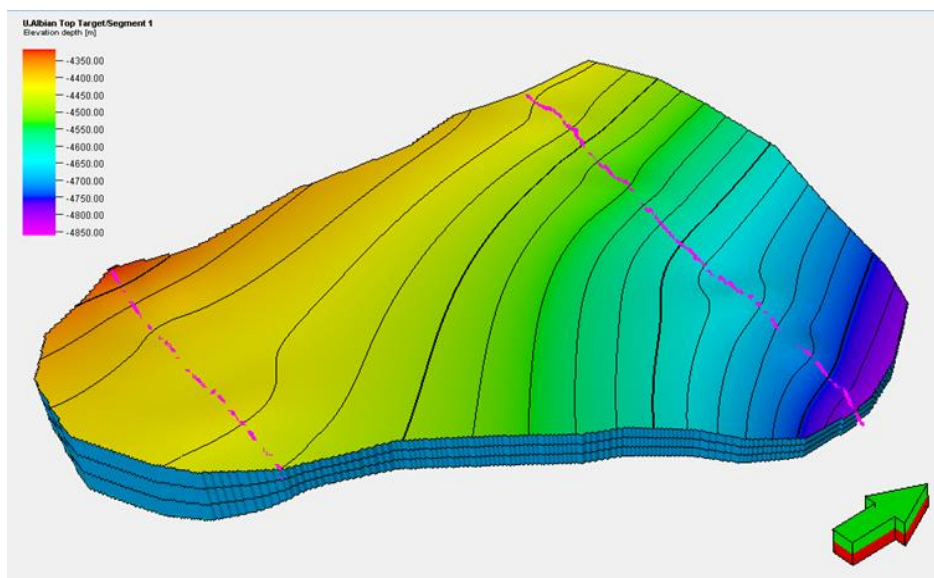
Figure 11: 3D structural model developed from structural maps in depth domain of the reservoir section with no faults associated.

The variations in thickness between top and base surfaces of the reservoir range from 12 m to 75 m. The southern part is thicker (50 - 75 m) compared to the rest of the area (Figure 12). The average thickness of the reservoir section is estimated to be ~50 m.
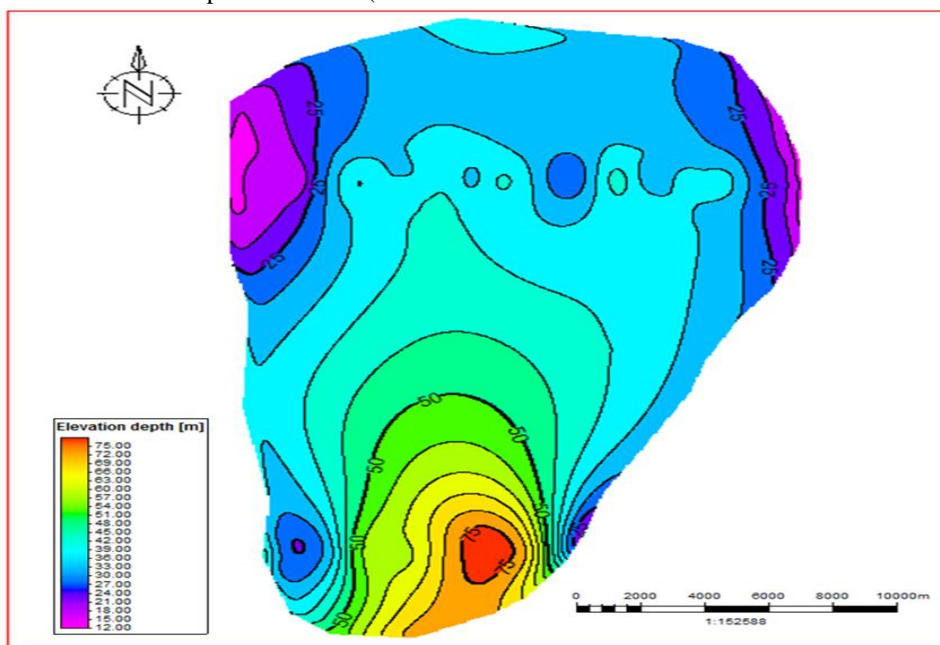
Figure 12: Thickness map of the reservoir structural model.

3D petrophysical property models
The porosity, permeability and water saturation curves were estimated from log analysis. Porosity curve reveals high values of up to > 25%, particularly in sandstone where the volume of shale is low than in the shale intercalation where shales dominate. The permeability curve reveals low values (less than 1 mD) and as it was observed in porosity, the higher values of permeability are covered by sandstone areas and the lower values are covered by the shale intercalations. Water saturation curve is generally observed to have higher values more than 65% whereby more water is carried in shale intercalations than in sandstone (Figure 13d). Other petrophysical parameters extrapolated using stochastic modeling technique revealed lithology distribution in most parts of the area is covered by sandstone facies for more than 60% intercalated by shale facies for less than 40% (Figure 13a). The porosity distribution model shows that the entire area of interest is mostly covered by high values of porosity ranging between 19% and 20% (Figure 13b). The permeability distribution model which honors the up-scaled well log data resulted into the entire area of interest being covered by low values of permeability between 1 and 10 mD, whereas most parts of the area fall at an average value of 6 to 7 mD (Figure 13c). The water distribution model shows that the entire area of interest is mostly covered by high values of water saturation of about 60% to 65% (Figure 13d).
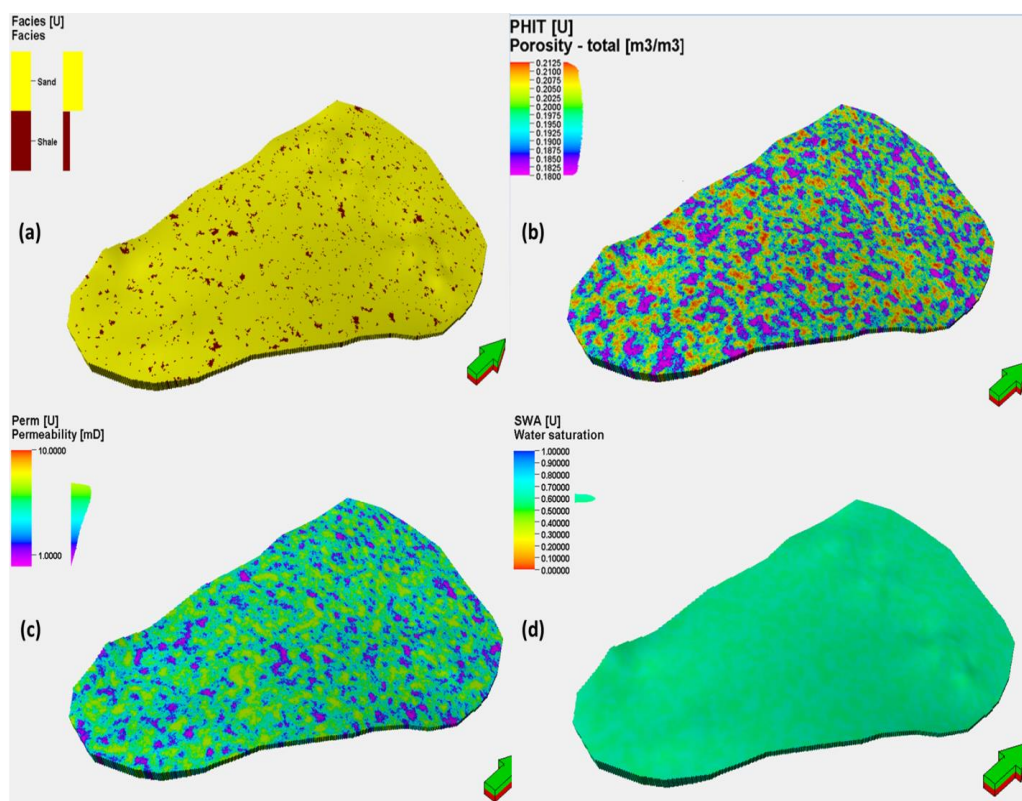
Figure 13: Petrophysical property models; (a) Lithology distribution model showing the spatial distribution of rock types, (b) Porosity distribution model, (c) Permeability distribution model and (d) Water saturation distribution model. The arrows point in the North direction.

Discussions

The time and depth structural contour maps configurations in Figure 8 and Figure 10 from seismic interpretations show that the reservoir section is typical a stratigraphic trap with no major or minor faults crossing the section as elaborated and references therein by Alvarenga et al. (2012) and Borgo et al. (2005). The chaotic textures of the seismic section around the reservoir section strongly reveal a marine slumped area similar to the findings by Schlaf et al. (2005) and Petrobras (2013). The 3D structural model also reveals that the target area for hydrocarbons is a stratigraphical trap (Figure 11) which is related to transgressive and regressive depositional sequence agreeing with Mbede (1991) and McDonough et al. (2013). No observed set of faults crossing the model except the traps made of lenses of deep water slumps and turbidities confirming the stratigraphical traps also described by Petrobras (2013) and Zongying et al. (2013).

The conventional log analysis showing high porosity between 19% and 20% in the static model in Figure 13 indicates the availability of enough pore spaces that can accommodate fluids resulted from well sorting of the grains, good packing of the grains and less compaction of the sediments during and after deposition as per similar findings by Halliburton (2001). The low permeability values of the reservoir section ranging from 6 to 7 mD suggest that the connection of the available pore spaces is poor due to reasons such as diagenesis whereby new minerals form between the pore spaces which block the passage after deposition. Both permeability and porosity values from the model rank the reservoir to a moderate to fairly quality reservoir based on the models by Levorsen (2001) and Adeoti et al. (2014). High water saturation values (60 – 65%) show that the percentage of hydrocarbons that occupy the pore spaces are insignificant compared to the percentage occupied by formation water and therefore the insignificant prospective accumulation of hydrocarbons in the reservoir section.

Conclusions

This study shows the usefulness of integrating 2D seismic reflection data with well log data in constructing a 3D geological reservoir model. The discrete and continuous well data gives the knowledge of the lithology in terms of the rock types and petrophysical properties of the area in terms of porosity, permeability and water saturation, while the 2D seismic data gives the knowledge of subsurface configuration of the reservoir section. The results of the petrophysical parameters of the Mafia Basin include 19-20% porosity, 6-7 mD permeability and 60-65% water saturation. These petrophysical parameters show that the area has moderate to a good quality reservoir hosted in stratigraphical traps but without significant hydrocarbon accumulation.

The 3D static model of the area has provided a better understanding of the spatial distribution of the discrete and continuous properties of the study area and the created geological model can be updated as more data are acquired for field development. Furthermore, this study recommends 3D seismic dataset and more number of wells in the future studies, to provide better analyses of the subsurface structural configuration and correlations to confirm the lateral continuity of the reservoir section. Besides, we also recommend follow-up detailed petrographic studies of core samples to calibrate the petrophysical values and reveal the digenetic history in the Mafia Basin, which is very important for hydrocarbon prospectivity.

References

Adeoti L, Onyekachi N, Olatinsu O, Fatoba J and Bello M 2014 Static reservoir modeling using well log and 3-D seismic data in a KN field, offshore Niger Delta, Nigeria. *Int. J. Geosc.* 5: 93-106.

Alvarenga NT, Nascimento MM, Etgeton VR, Couto N and Fonseca JP 2012 Final geological report, zeta-1 well, block 5 offshore Tanzania. Petrobras Tanzania.

Archie GE 1942 The electrical resistivity log as an aid in determining some reservoir characteristics. *Trans. AIME* 146(01): 54-62.

Bjorlykke K 2010 Petroleum Geoscience: From Sedimentary Environments to Rock Physics. 1st ed., Springer Science & Business Media.

Borgo HG, Skov T and Sønneland L 2005 Automated structural interpretation through classification of seismic horizons. In: Iske A, Randen T (eds) *Mathematical Methods and Modelling in Hydrocarbon Exploration and Production. Mathematics in Industry* Vol 7 (pp. 89-106). Springer, Berlin, Heidelberg.

Branets LV, Ghai SS, Lyons SL and Wu XH 2009 Challenges and technologies in reservoir modeling. *Comm. Comput.Phys.* 6: 1-23.

Cope MJ 2000 Tanzania's Mafia deep water-basin indicates potential on new seismic data. *Oil & Gas Journal* 98(33): 40-49.

Christie MA and Blunt MJ 2001 Tenth SPE comparative solution project: A comparison of upscaling techniques. In: *SPE Reservoir Simulation Symposium.* Society of Petroleum Engineers.

Cunningham AD and Droxler AW 2000 Synthetic seismogram generation and seismic facies to core lithology correlation for Sites 998, 1000, and 1001. In *Proceeding of the Ocean Drilling Program, Scientific Results* 165: 205-217.

Deutsch CV 1992 *Annealing techniques applied to reservoir modeling and the integration of geological and engineering (well test) data*. PhD dissertation, Stanford University.

Farmer CL 2005 Geological modelling and reservoir simulation. In *Mathematical methods and modelling in hydrocarbon exploration and production* (pp. 119-212). Springer, Berlin, Heidelberg.

Gluyas J and Swarbrick R 2003 Petroleum Geoscience. John Wiley & Sons.

Halliburton AD 2001 Basic Petroleum Geology and Log Analysis. Halliburton *Company*.

Harris PM and Weber LJ (Eds) 2006 Giant hydrocarbon reservoirs of the world: from rocks to reservoir characterization and modeling. *AAPG Memoir* 88: 307-353.

Harris DG 1975 The role of geology in reservoir simulation studies. *J. Petrol. Technol.* 27(5): 625-632.

Holden L and Nielson BF 2000 Global Upscaling of permeability in heterogeneous reservoirs: The output least squares (ols) method. *Transp. Por. Med.* 40 (2): 115-143.

Hu LY 2000 Gradual deformation and iterative calibration of Gaussian-related stochastic models. *Math. Geol.* 32(1): 87-108.

Kent PE, Hunt JA and Johnstone DW 1971 The Geology and Geophysics of Coastal Tanzania. Geophysical 6. HMS Stationary Office, Institute of Geophysical Sciences, London, 101.

Levorsen AI 2001 Geology of Petroleum. 2nd ed, The AAPG Foundation.

Mbede EI 1991 The sedimentary basins of Tanzania-reviewed. *J. Afr. Earth Sci. (Mid. East)* 13(3-4): 291-297.

McDonough KJ, Bouanga E, Pierard C, Horn B, Emmet P, Gross J, Danforth A, Sterne N and Granath J 2013 Wheeler-transformed 2D seismic data yield fan chronostratigraphy of offshore Tanzania. *Lead. Edge* 32(2): 162-170.

Merletti G and Torres-Verdin C 2006 Accurate detection and spatial delineation of thin-sand sedimentary sequences via joint stochastic inversion of well logs and

3D pre-stack seismic amplitude data. In *SPE Annual Technical Conference and Exhibition*. Society of Petroleum Engineers.

Nicholas CJ, Pearson PN, McMillan IK, Ditchfield PW and Singano JM 2007 Structural evaluation of southern coastal Tanzania since the Jurassic. *J. Afr. Earth Sci.* 48(4): 273-297.

Nikravesh M and Aminzadeh F 2001 Past, present and future intelligent reservoir characterization trends. *J. Petro. Sci. Engin.* 31(2-4): 67-79.

Pereira-Rego M, Carr AD and Cameron NR 2013 Gas Success along the margin of East Africa, but where is all the generated oil? American Association of Petroleum Geologists (AAPG) Online Journal for E&P Geoscientists; *Adapted from a presentation given at the East Africa Petroleum Province of the 21st Century Conference, October 24-26, 2012, The Geological Society, London, England*. http://www.searchanddiscovery.com/pdfz/documents/2013/10488pereira/ndx_pereira.pdf.html

Petrobras 2013 Block 5 Relinquishment Report: Technical Evaluation of Exploration Potentials of Block 5, Offshore Tanzania (Unpublished).

Petzet A 2012 Deepwater, land discoveries high-grade East African margin. *Oil Gas J.* 110(4): 70-70.

Pyrcz MJ and Deutsch CV 2014 Geostatistical Reservoir Modeling. 2nd ed, Oxford University Press, New York.

Ringrose P and Bentley M 2015 The property model. In: *Reservoir Model Design* (pp. 61-113). Springer Dordrecht.

Schlaf J, Randen T, Sønneland L 2005 Introduction to seismic texture. In: *Mathematical Methods and Modelling in Hydrocarbon Exploration and Production* (pp. 3-21). Springer, Berlin, Heidelberg.

Schlumberger 2014 Petrel, Geology and Geophysics User Guide. *Schlumberger.*

Slind OL, DuToit SR and Kidston AG 1998 The Hydrocarbon potential of the East Africa continental margin. Pet. Explor. Dev., pp. 436-437.

Soleimani M and Shokri BJ 2015 3D static reservoir modeling by geostatistical techniques used for reservoir characterization and data integration. *Environ. Earth Sci.* 74(2): 1403-1414.

Seifert D and Jensen JL 1999 Using sequential indicator simulation as a tool in reservoir description: Issues and uncertainties. *Mathematical Geology* 31(5): 527-550.

Timur A 1968 An investigation of permeability, porosity & residual water saturation relationships for sandstone reservoirs. *Log Anal.* 9(04).

Zongying Z, Ye T, Shujun L and Wenlong DING 2013 Hydrocarbon potential in the key basins in the East Coast of Africa. *Petrol. Explor. Dev.* 40(5): 582-591.